NANO LETTERS

2007
Vol. 7, No. 12
3662−3668

Two-Dimensional Confinement of Nanorods in Block Copolymer Domains

Ranjan D. Deshmukh,† Yu Liu,† and Russell J. Composto*

Department of Materials Science and Engineering and Laboratory for Research on the Structure of Matter, University of Pennsylvania, Pennsylvania 19104-6272

Received August 3, 2007; Revised Manuscript Received October 14, 2007

ABSTRACT

Gold nanorods (NRs) self-orient during the self-assembly of a symmetric poly(styrene-b-methyl methacrylate) (PS-b-PMMA) film. The NRs are selectively sequestered and confined in lamellar PMMA domains, which are narrower than the NR length. This confinement orients 71% of NRs within ± 5° of the lamella plane. During solvent annealing, a gradient in the concentration of NRs is observed. This route to produce alternating layers containing conducting NRs separated by dielectric domains has the potential for fabricating self-assembled nanodevices.

By combining nanoparticles (NPs) with complementary matrix materials, nanoscale devices can be devised with properties that make them suitable for electronic[1,2] and optoelectronic devices,[3−5] magnetic storage,[6] biomedical applications,[7,8] and catalysis.[9] NPs can be produced with a wide range of shapes, including sphere, pyramid, cubic, rod, and branched rod, which can significantly affect the device properties and sensitivity. For example, photovoltaic devices (solar cells) constructed from branched nanorods (NRs) of cadmium selenide, CdSe, mixed with a conjugated polymer showed enhanced efficiency compared to NRs of CdSe dispersed in the same polymer.[4] NP shape also impacts optical properties as noted by the observation of two plasmon resonance peaks, transverse and longitudinal, for gold NRs, whereas spherical NPs displayed only a single peak.[10] Mechanical properties of nanocomposites are also sensitive to NP shape. Simulations showed that NR partitioning into the minority phase of a polymer blend could result in a bicontinuous morphology with a percolated network of NRs and enhanced mechanical properties.[11]

The assembly of one-dimensional (1D) objects in layered structures is of broad interest as noted by previous studies of DNA insertion in liposome complexes.[12−16] For nanoscale devices that utilize elongated NPs (e.g., nanowire transistors), a significant challenge is to control the orientation and packing of the NPs. For example, aligned gold NRs and silver nanowires exhibited a localized surface plasmon resonance, which is useful for surface-enhanced Raman spectroscopy (SERS) and probing the local dielectric environment (i.e., chemical sensors).[17−20] In addition to the aspect ratio of the NP, the enhanced SERS signal depended on the lateral arrangement or packing of NRs. By applying an electric field during solvent evaporation, cadmium sulfide, CdS,[21] and CdSe[22] NRs were observed to align and form a close-packed structure. Other methods for controlling NR orientation include stretching polymer films containing NRs,[23,24] electron beam lithography with a lift-off technique,[18,19] deposition on chemically patterned substrates,[25] and optical trapping via laser radiation.[26] Alignment of a monolayer of silver nanowires on silicon was also achieved using the Langmuir−Blodgett technique.[17,27] In a recent breakthrough, In_2O_3 and ZnO nanowires were deposited from suspension onto a gate-patterned flexible substrate to create an optically transparent and mechanically flexible device.[28] Although this is a significant step toward developing next generation displays, experiments aimed at controlling the organization of nanowires/NRs are necessary to enable the creation of arrays of individually addressable nanocomponents that make up devices.

In the present study, the orientation of NRs is achieved by preferentially confining them in a particular domain of a symmetric diblock copolymer that forms a lamellar morphology. Several research groups have investigated the self-assembly of spherical NPs on a surface[29−32] and in the bulk of block copolymer films.[33−42] However, studies involving the self-assembly of block copolymers containing nonspherical NPs are relatively recent. Russell and co-workers deposited CdSe NRs modified with poly(ethylene oxide), PEO, from an aqueous solution onto the surface of poly(styrene-b-MMA), PS-b-PMMA, films having a perpendicular lamellar morphology of alternating PS and PMMA stripes.[43] Because of an attractive interaction between the PEO brush and PMMA block, the CdSe NRs located selectively on the PMMA stripes. Laicer et al.[44,45] showed that gold NRs added to poly(S-b-isoprene), PS-b-PI, seed

* To whom correspondence should be addressed. Telephone: 215-898-4451. Fax: 215-573-2128. E-mail: composto@seas.upenn.edu.
† These authors contributed equally to this work.

10.1021/nl071908r CCC: $37.00
Published on Web 11/23/2007

the growth and orientation of cylindrical domains. Chen et al. simulated the self-assembly of a diblock copolymer/NR mixture where NRs were attracted to one of the blocks.[46] Because this attraction drove the NRs into the confining domain, the NRs underwent a nematic ordering transition.[46]

This study investigates the self-assembly of a symmetric block copolymer, PS-b-PMMA, containing gold NRs modified with a poly(ethylene glycol), PEG, brush. Thus, our study differs from those designed to understand the self-assembly of NRs on the surface of a block copolymer.[43] The average NR length and diameter are 0.71 and 0.27*L*, respectively, where *L* is the lamella period of the copolymer. These NRs segregate to the PMMA domains (width $\sim 0.5L$) because of the favorable interaction between the PEG brush and PMMA block. For the first time, our experiments demonstrate in a quantitative fashion that a majority of NRs orient with their long axis parallel to lamellae due to confinement by narrow PMMA domains. Further we show that solvent annealing produces a gradient in the NR concentration within the block copolymer films and a dense array of NRs adjacent to the substrate.

The copolymer is PS-b-PMMA with molecular weight, $M_w = 211$ kg/mol, and PDI = 1.13 (Polymer Sources Inc.). The volume fraction of PMMA is 0.48 and lamellae period, $L \sim 67.2$ nm.[47] Chloroauric acid trihydrate, cetyltrimethylammoniumbromide (CTAB), L-ascorbic acid, sodium borohydride, silver nitrate, *O*-[2-(3-mercaptopropionylamino)-ethyl]-*O′*-methylpoly(ethylene glycol) or PEG-thiol (5000 g/mol), toluene, and methanol were purchased from Sigma-Aldrich and used as received. Water was obtained from a water purification system (Millipore).

Gold NRs were synthesized following the method developed by Murphy et al.[48] For gold seed synthesis, 250 μL of a 0.01 M $HAuCl_4 \cdot 3H_2O$ solution was added to 7.5 mL of a 0.1 M CTAB solution followed by the addition of 600 μL of ice-cold 0.01 M $NaBH_4$ with rapid inversion mixing for 2 min. The gold NRs were grown by adding appropriate quantities of reagents to a plastic centrifuge tube in the order of CTAB, $HAuCl_4 \cdot 3H_2O$, $AgNO_3$, ascorbic acid, and the seed solution. In a typical experiment, 120 mL of 0.1 M CTAB, 5.1 mL of 0.01 M $HAuCl_4 \cdot 3H_2O$, 0.75 mL of 0.01 M $AgNO_3$, and 0.81 mL of a 0.1 M ascorbic acid solution were added in the same order followed by gentle mixing after each step. Finally, 1.26 mL of seed solution was added, and left undisturbed for at least 3 h.

The NRs were modified with PEG-thiol according to the method described by Sönnichsen et al.[49] The excess CTAB in the as-prepared NRs was removed by two centrifugation cycles followed by redispersion of the NRs in ultrapure water. A 7.2 mL sample of fresh 2 mM PEG-thiol was then added to the surfactantless NR solution. The reaction mixture was incubated and shaken at room temperature for 2 h. Finally, the PEG functionalized NRs, PEG-NR, were purified via a centrifuge and redispersed first in methanol and then in toluene for further use.

PS-b-PMMA powder was added to 1 mL of PEG-NR/toluene to make a 1 wt % polymer solution. The concentration of the NRs in PS-b-PMMA was calculated to be 5 vol %. This solution was filtered (pore size, 0.25 μm) to obtain a clear solution without any visible aggregates or suspended impurities. The films were solution cast on silicon, glass, and epoxy substrates. These substrates were cleaned with acetone and toluene and then were dried under a N_2 stream. To create hydroxyl groups on the silicon, silicon substrates were immersed in a piranha solution (7:3 v/v, 98% H_2SO_4/30% H_2O_2) for 30 min at 80 °C. Next, these substrates were rinsed with ultrapure water, dried with a N_2 stream and exposed to UV−ozone for 10 min before casting polymer films on the substrates. The filtered NR/polymer solution was deposited on the substrates and allowed to evaporate in a saturated toluene vapor for 2 days. After this "solvent annealing" step, the films were dried overnight in a fume hood and then in a vacuum oven for 1 day at room temperature. The resulting nanocomposite films were about 0.5−2 μm thick. Thin films (43 nm) were prepared by spin-coating (2000 rpm) the same solution on glass substrates and then solvent annealed following the above procedure. Solvent annealing of the PEG-NR/PS-b-PMMA films was used to allow the block copolymer to self-assemble and NRs to migrate. Thermal annealing could not be used because Au-NRs have been found to reshape upon thermal annealing above 100 °C.[50]

The NR shape, size, and location in the lamellar PS-b-PMMA morphology were determined by transmission electron microscopy (TEM, JEOL 2010). Images were taken at 80 kV to minimize degradation of PMMA. For imaging the PEG-NR, a few drops of the NR/methanol solution was deposited on holey carbon-coated grids (mesh size 300, SPI supplies). For imaging the nanocomposite films, cross-sections (∼50−70 nm) were prepared by ultramicrotomy (Richtheart Jung Ultramicrotome) on solvent-annealed films deposited on an epoxy substrate. ImageJ 1.37 software (NIH, USA) was used to process TEM images to determine NR size and orientation with respect to the lamellae. The 43 nm thin films were floated off in ultrapure water from glass substrates and picked up on carbon-coated copper grids for TEM imaging.

Rutherford backscattering spectrometry (RBS, NEC Corporation 5 SDH Pelletron) was used to depth profile gold in the nanocomposite films. For this study, a 2 MeV $^4He^+$ ion beam was incident at 10° with respect to the sample surface. The total charge was 4 μC. RUMP software (Genplot) was used to simulate RBS spectra and convert the energy scale to depth. The optical properties of the NRs were studied by UV−visible spectroscopy (Varian, Cary 5000 UV−visible spectrophotometer).

Before blending with the block copolymer, the NRs were characterized by TEM. Figure 1a shows the TEM image of PEG-NR (only the gold core is visible). Although some cubes and other shapes are observed, about 90% of the NPs are NRs. The formation of cubes and other shapes as well as the curvature of the NRs and cubes are consistent with previous studies.[48] To obtain statistically significant values, 176 NRs were analyzed to determine the average length and diameter. Figure 1b shows the size distribution of the length and diameter of the gold core. The average length and

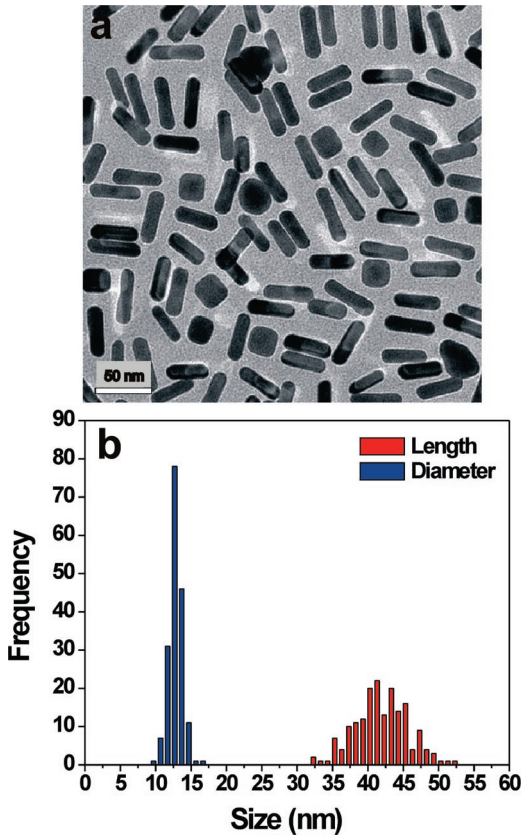

Figure 1. (a) TEM image of PEG-NR on a holey carbon-coated grid. (b) Size distribution of NR dimensions (length and diameter).

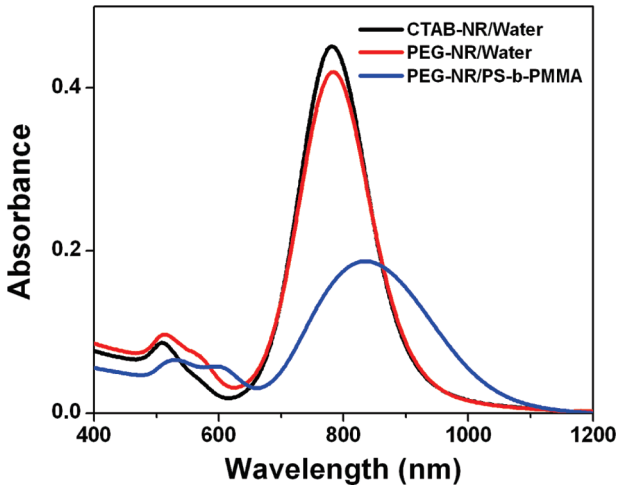

Figure 2. UV-vis absorbance spectra of CTAB-NR and PEG-NR dispersed in water and PEG-NR/PS-b-PMMA film.

diameter of the gold core were 42.1 ± 3.7 and 12.6 ± 1 nm with an average aspect ratio of about 3.3. Assuming that the PEG brush layer thickness is equal to the unperturbed radius of gyration, 2.8 nm,[51] the overall NR dimensions are 47.7 nm × 18.2 nm, respectively.

The optical properties of the CTAB functionalized NRs (CTAB-NR) and PEG-NR in water as well as the PEG-NR (5 vol %)/PS-b-PMMA film (43 nm) on glass were measured by UV−vis spectroscopy as shown in Figure 2. All spectra show two plasmon resonance bands located at short and long wavelengths corresponding to the transverse and longitudinal excitation modes along the NR, respectively. The plasmon resonance peak position depends on type, size, shape of the NPs and refractive index or dielectric constant of the surrounding medium.[52] Upon replacing CTAB with PEG, the transverse and longitudinal plasmon peaks undergo small red shifts from 510 to 514 nm and 781 to 784 nm, respectively, which is due to the thin PEG coating on the NRs.[53] Upon changing the medium of the PEG-NR from water to PS-b-PMMA, the short and long wavelength peaks undergo strong red shifts from 514 to 531 nm and 784 to 836 nm, corresponding to 17 and 52 nm, respectively. Wang et al. found a red shift in peak position of NRs as the local refractive index of the media increased.[54] For PEG-NR, the observed red shift in peak position upon changing the dispersing medium from water to copolymer is consistent with an increase in refractive index in the visible spectrum range from 1.33 for water[55] to ∼1.44 for PS-b-PMMA (i.e., 1.59 and 1.49 for PS and PMMA,[56] respectively). Figure 2 also shows that the short wavelength peaks have shoulders near 560 and 595 nm for samples in water and polymer film, respectively, which correspond to plasmon resonance associated with the nanospheres, nanocubes, and other shaped NPs.[57]

The PEG-NR (5 vol %) were incorporated in PS-b-PMMA films and cross-sections of the nanocomposite films were imaged by TEM as shown in Figure 3a. Upon solvent annealing for 2 days, the PS-b-PMMA film self-assembles into lamellae (Figure 3a) parallel to the epoxy substrate. Kim et al.[37] showed that high loadings of spherical NPs could cause a transition from lamellar to other morphologies (e.g., spherical) in block polymer films. To observe a lamellar to cylinder transition in our system, one would need to add about 34 vol % of NRs, which is much higher than the experimental loading. The contrast between PS (dark) and PMMA (bright) domains is due to the degradation of PMMA block under the electron beam. Figure 3a shows that individual and small assemblies of NRs are uniformly distributed throughout the film, except for a monolayer of NRs that have segregated to the substrate during solvent annealing. Taken at a higher magnification, Figure 3b shows that the NRs have selectively localized in the PMMA domains (bright) and predominantly orient with their long axis parallel to the lamellae. The NR localization in PMMA results from a favorable interaction between the PEG brush and the PMMA block, consistent with experiments by Russell et al.[43] and simulations by Chen et al.[46] Because the cross-sectional TEM images (Figures 3a,b) show a 2D projection, the azimuthal orientation of NRs (ϕ, defined in Figure 4a) within the PMMA lamellae is not observed. Namely, the NRs could be randomly oriented ($-180° < \phi < 180°$) within the PMMA lamellae. This suggestion is supported by the observation that the projected lengths of the NRs (cf., Figure 3b) are either shorter than or equal to actual length (Figure 1a). To verify this interpretation, Figure 3c shows a top view of a solvent-annealed film (43 nm) that displays randomly oriented NRs (azimuthally) within the lamellae. The NRs in the as-cast film also showed random orientations similar to Figure 3c.

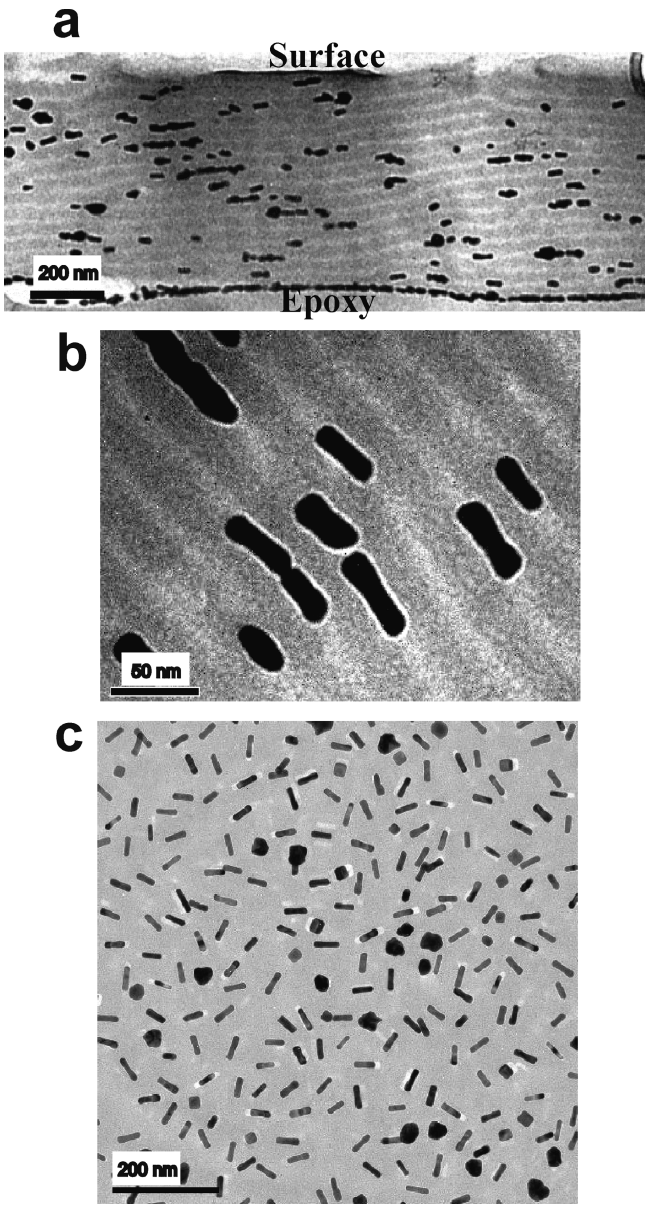

Figure 3. (a) Cross-sectional TEM image of solvent-annealed PEG-NR/PS-b-PMMA film. Dark and light stripes represent PS and PMMA, respectively. (b) Higher magnification TEM image of the nanocomposite film showing NRs oriented within PMMA lamellae. (c) Top-down view of a solvent-annealed PS-b-PMMA film (43 nm).

On the basis of the TEM images (e.g., Figure 3), the 3D and 2D projections of the NRs can be determined and defined using spherical coordinates. Figure 4a shows the 3D NRs (dark gold) randomly oriented within PMMA domains (red) as well as their projection in 2D (brown). The orientation of the 3D NR with respect to the lamellae plane (i.e., $x-y$ plane) is defined as θ, whereas the orientation of the 2D NR along the $x-z$ plane is θ' as shown in Figure 4a. The angle θ reflects the degree of NR confinement imposed by the PMMA domain, where a perfectly oriented NR corresponds to $\theta = 0°$. To relate θ' measured by TEM to θ, the geometric relationship, $\sin(\theta) = (\text{projected length}/42.1) \times \sin(\theta')$, is used, where 42.1 is the measured length of the gold core (cf., Figure 1b). About 145 NRs within the bulk of the films

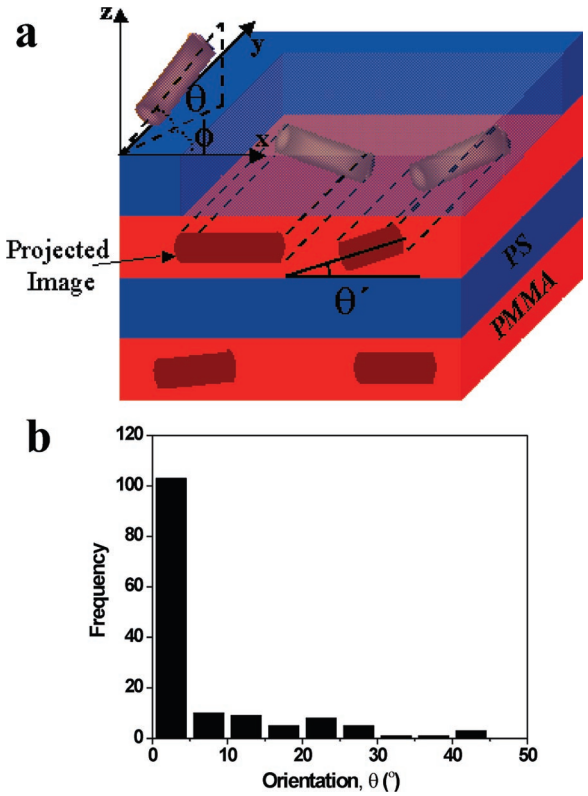

Figure 4. (a) Schematic of NRs within the lamellar PMMA domains of a PS-b-PMMA film. The schematic shows the actual (3D) and projected (2D) images of the NRs. The PS and PMMA are blue and red, respectively, whereas the 3D and 2D images are dark gold and brown, respectively. The definitions of azimuthal angle, ϕ, NR orientation, θ, and orientation of the projected image, θ', are also shown. (b) Distribution of NR orientation (θ) with respect to the lamellae. Frequency represents the number of NRs oriented within a 5° window.

were analyzed. Figure 4b shows how the number of NP or frequency varies with θ over 5° increments, $0-5°$, $5-10°$, and so on. A key result is that 71% of the NRs are strongly oriented with their long axis parallel to the lamellae, namely $-5° \leq \theta \leq 5°$. Correspondingly, about 78 and 88% of the NRs are oriented within $\pm$ 10 and $\pm$ 20°, respectively.

NR orientation imposed by the block copolymer domains is an important outcome of this study. The molecular weight of the symmetric PS-b-PMMA was chosen such that the PMMA domain width ~34 nm ($L/2$) was greater than the PEG-NR diameter, 18.2 nm, but less than the PEG-NR length, 47.7 nm. By a geometric argument, the PEG-NR can be shown to fit within the PMMA domain if $\theta \leq 21°$. For $\theta > 21°$, a portion of the PEG-NR would penetrate into the PS domain resulting in an enthalpic penalty due to the unfavorable PS/PEG interaction. The analysis of PEG-NR orientation given in Figure 4b shows that only about 12% of the NRs satisfy $\theta > 21°$, indicating that the enthalpic penalty is significant. Taken alone, this enthalpic argument would predict that all NR orientations are equally probable if they satisfy $\theta \leq 21°$. However, Figure 4b shows that the NRs clearly have a preferred orientation with respect to the lamellae. The conformational entropy of the PMMA brush may account for this behavior. Figures 5a,b describe the molecular conformations after a NR (gold) is inserted in the

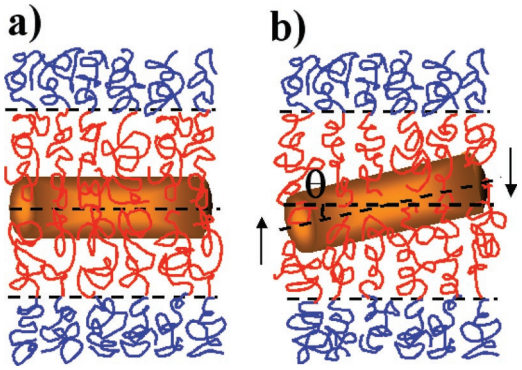

Figure 5. A molecular model showing chain deformation after a NR is inserted in the PMMA domain of PS-b-PMMA lamellae. Two cases are shown with NR oriented at (a) 0° and (b) θ° with respect to the lamellae. The arrows in (b) denote the direction of the force exerted on the NR due to compression and stretching of the polymer chains in the vicinity of the NR. The color scheme for the PS block, PMMA block, and NR is blue, red, and gold, respectively.

PMMA domain (red) at $\theta = 0°$ or an angle between $\pm 21°$, respectively. The pressure due to the PMMA brush acting at a distance z from the PS/PMMA interface ($z = 0$) is given by[58]

$$P(z) \propto (h^2/N^2)(1 - z^2/h^2) \quad (1)$$

where h is the height of the brush (i.e., $L/4$), and N is the degree of polymerization of PS-b-PMMA. The entropic energy cost, $F(z)$, is given by[58]

$$dF(z) \sim P(z)^* dV \quad (2)$$

where dV is the differential volume of the NR at distance z. To accommodate the inserted NR, PMMA chains would have to stretch or contract to fill space around the NR, as demonstrated in Figure 5b. This deformation would produce a pressure (eq 1) and thus entropic energy penalty (eq 2), relative to the case shown in Figure 5a. Thus, we attribute the strong orientation of NRs presented in Figure 4b to the entropic penalty associated with deforming the PMMA chains surrounding the NR.

Experiments were performed to determine whether stratification observed in TEM studies (cf., Figure 3a) resulted from NR attraction for the substrate or their partitioning during solvent annealing. Films of PEG-NR/PS-b-PMMA were prepared by solvent annealing on epoxy, glass, silicon (Si), and hydroxyl-terminated silicon (Si−OH) substrates. Using RBS, the depth profile of gold is determined, and the spectra for films deposited on the glass, Si, and Si−OH are shown in Figure 6. For all substrates, the gold concentration is low at the surface, moderate in the middle of the film, and highest near the substrate. The peaks indicate that the NR concentration is enriched near the interface of the three different substrates. The peak positions are shifted because the film thickness values differ, namely, 1.75, 1.6, and 1.87 μm on glass, Si, and Si−OH, respectively. Although ion beam charging prevents RBS studies of films on epoxy, the

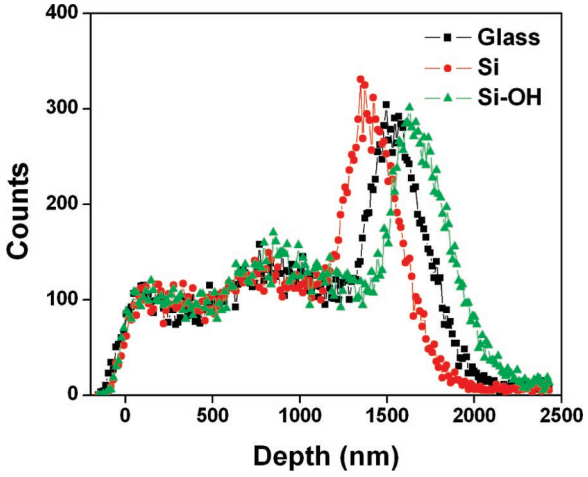

Figure 6. Rutherford backscattering spectra showing the depth profile of gold in solvent-annealed PS-b-PMMA films on glass, Si, and Si−OH substrates. The counts are proportional to the gold concentration in the PS-b-PMMA films.

TEM images of film cross-sections taken on epoxy substrates (e.g., Figure 3a) are consistent with the RBS spectra for glass, Si, and Si−OH, suggesting that the enrichment of NRs is independent of the substrate type. Thus, the NR interaction with the substrate is an unlikely driving force for the NR enrichment near the substrate.

The NR concentration gradient in the film and enrichment near the substrate most likely occur during solvent evaporation. Figure 7 represents how NRs may partition during the early, intermediate, and final stages of solvent annealing. Initially, NRs are uniformly dispersed throughout the polymer solution (~1 wt % PS-b-PMMA) deposited on the substrate (Figure 7a). Because evaporation from the near surface region is relatively fast, the solvent concentration is low near the surface and increases toward the substrate during drying (Figure 7b). Previously, Russell et al.[59] demonstrated that a solvent gradient exists during slow solvent evaporation from PS-b-PEO films. Thus, we propose that NRs are rejected from the near surface region (i.e., concentrated solution) toward the substrate (i.e., dilute solution). An analogous phenomenon is observed in the solidification of one-phase metal alloys where solute is rejected from the solid phase into the liquid phase.[60] The origin of NR rejection from the concentrated solution may derive from a reduction in the conformational entropy of block copolymer chains as well as the combinatorial entropy contribution. This behavior is represented by Figure 7b, which shows a high concentration of NRs in the solvent-rich region adjacent to the substrate. After complete solvent evaporation, a dry film is produced with a gradient in NR concentration and NR enrichment near the substrate as shown in Figure 7c. In very thick films (100 μm) of block copolymer, Kim et al.[37] previously reported a gradient of NP concentration upon solvent annealing. Although their NP profile differs from ours, the proposed mechanism qualitatively predicts the NR gradient in our film.

Solvent evaporation may also explain the NR concentration profile across the film, as shown in Figure 6. Specifically, a nonuniform rate of solvent evaporation may produce this variation in concentration. Initially, rapid evaporation from

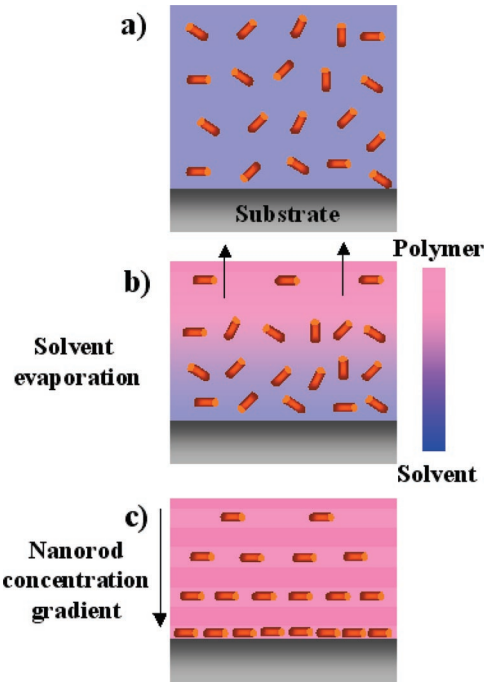

Figure 7. (a) NRs uniformly dispersed in a solution drop cast on a substrate. (b) Solvent evaporation from the near-surface region (arrows) creates a gradient in solvent concentration leading to a rejection of NRs toward the substrate. (c) After drying, the block copolymer is ordered and a gradient in NR concentration is observed with enrichment near the substrate. The reference color bar ranges from pink and dark blue, which corresponds to pure polymer and solvent, respectively. Intermediate colors represent a mixture of polymer and solvent.

the surface can immobilize NRs such that the concentration near the surface is greater than just below the surface, a result supported by the surface peak in Figure 6. This "skin" will allow the region below the surface to dry slowly, allowing for NR rejection toward the substrate. Following the analogy with alloy solidification, the rejected rods "pile up" on the solvent-rich side and, simultaneously, a drying front passes through this region and freezes the NRs. This explanation is consistent with the observed increase in NR concentration about 900 nm below the surface of films deposited on various substrates (cf., Figure 6). The NRs continue to get rejected toward the substrate, and upon complete drying enrich the substrate as previously described. To determine whether the observed step in concentration (near 900 nm) is due to a variation in film thickness, scanning force microscopy images were taken (50 μm $\times$ 50 μm) and show an average height variation of only 60 nm. A much larger thickness variation of $\sim$1000 nm is needed to reproduce the step shown in Figure 6. Although we have also observed a similar concentration profile of NRs in a cylindrical morphology, further studies, for example, solvent annealing with controlled solvent vapor pressure, are required before a detailed understanding is possible.

In summary, this study demonstrates that PEG-NR can be selectively partitioned in the lamellar PMMA domains in PS-b-PMMA film. By choosing an appropriate lamellar width relative to NR dimensions, the orientation of the NRs within PMMA domains can be controlled. We show for the first time that the majority of NRs are oriented with their long axis parallel to the lamellae due to confinement effects. Solvent annealing is shown to create a gradient in NR concentration across the polymer as well as an enrichment of NRs adjacent to the substrate. This concentration gradient results from the rapid evaporation of solvent from the near surface region as compared to regions near the substrate and thereby entropic rejection of NRs toward the substrate.

Acknowledgment. This work was funded by the National Science Foundation Polymer (DMR05-49307), MRSEC (DMR05-20020), and NSEC (DMR04-25780) programs, as well as the ACS/PRF program (43616-AC7). We gratefully acknowledge the use of microtome in Prof. K. Winey's laboratory at the University of Pennsylvania.

References

(1) Matsui, I. *J. Chem. Eng. Jpn.* **2005**, *38* (8), 535−546.
(2) Tseng, R. J.; Tsai, C. L.; Ma, L. P.; Ouyang, J. Y. *Nat. Nanotech.* **2006**, *1* (1), 72−77.
(3) Konstantatos, G.; Howard, I.; Fischer, A.; Hoogland, S.; Clifford, J.; Klem, E.; Levina, L.; Sargent, E. H. *Nature* **2006**, *442* (7099), 180−183.
(4) Sun, B.; Marx, E.; Greenham, N. C. *Nano Lett.* **2003**, *3* (7), 961−963.
(5) Liu, J. S.; Tanaka, T.; Sivula, K.; Alivisatos, A. P.; Frechet, J. M. J. *J. Am. Chem. Soc.* **2004**, *126* (21), 6550−6551.
(6) Gas, J.; Poddar, P.; Almand, J.; Srinath, S.; Srikanth, H. *Adv. Funct. Mater.* **2006**, *16* (1), 71−75.
(7) Brannon-Peppas, L.; Blanchette, J. O. *Adv. Drug Delivery Rev.* **2004**, *56* (11), 1649−1659.
(8) Kaittanis, C.; Naser, S. A.; Perez, J. M. *Nano Lett.* **2007**, *7* (2), 380−383.
(9) Jaramillo, T. F.; Baeck, S. H.; Cuenya, B. R.; McFarland, E. W. *J. Am. Chem. Soc.* **2003**, *125* (24), 7148−7149.
(10) Murphy, C. J.; Sau, T. K.; Gole, A.; Orendorff, C. J. *MRS Bull.* **2005**, *30* (5), 349−355.
(11) Buxton, G. A.; Balazs, A. C. *Mol. Simul.* **2004**, *30* (4), 249−257.
(12) Joachim, O. R.; Koltover, I.; Salditt, T.; Safinya, C. R. *Science* **1997**, *275* (5301), 810−814.
(13) Safinya, C. R. *Curr. Opin. Struc. Biol.* **2001**, *11* (4), 440−448.
(14) Bruinsma, R.; Mashl, J. *Europhys. Lett.* **1998**, *41* (2), 165−170.
(15) Dan, N. *Biophys. J.* **1997**, *73* (4), 1842−1846.
(16) Dan, N. *Biochim. Biophys. Acta* **1998**, *1369* (1), 34−38.
(17) Tao, A.; Kim, F.; Hess, C.; Goldberger, J.; He, R. R.; Sun, Y. G.; Xia, Y. N.; Yang, P. D. *Nano Lett.* **2003**, *3* (9), 1229−1233.
(18) Ueno, K.; Mizeikis, V.; Juodkazis, S.; Sasaki, K.; Misawa, H. *Opt. Lett.* **2005**, *30* (16), 2158−2160.
(19) Ueno, K.; Juodkazis, S.; Mino, M.; Mizeikis, V.; Misawa, H. *J. Phys. Chem. C* **2007**, *111* (11), 4180−4184.
(20) Yang, Y.; Xiong, L. M.; Shi, J. L.; Nogami, M. *Nanotechnology* **2006**, *17* (10), 2670−2674.
(21) Ryan, K. M.; Mastroianni, A.; Stancil, K. A.; Liu, H. T.; Alivisatos, A. P. *Nano Lett.* **2006**, *6* (7), 1479−1482.
(22) Gupta, S.; Zhang, Q. L.; Emrick, T.; Russell, T. P. *Nano Lett.* **2006**, *6* (9), 2066−2069.
(23) van der Zande, B. M. I.; Pages, L.; Hikmet, R. A. M.; van Blaaderen, A. *J. Phys. Chem. B* **1999**, *103* (28), 5761−5767.
(24) Murphy, C. L.; Orendorff, C. J. *Adv. Mater.* **2005**, *17* (18), 2173−2177.
(25) Liu, S. H.; Tok, J. B. H.; Locklin, J.; Bao, Z. N. *Small* **2006**, *2* (12), 1448−1453.
(26) Pelton, M.; Liu, M. Z.; Kim, H. Y.; Smith, G.; Guyot-Sionnest, P.; Scherer, N. E. *Opt. Lett.* **2006**, *31* (13), 2075−2077.
(27) Chung, S. W.; Markovich, G.; Heath, J. R. *J. Phys. Chem. B* **1998**, *102* (35), 6685−6687.
(28) Ju, S. Y.; Facchetti, A.; Xuan, Y.; Liu, J.; Ishikawa, F.; Ye, P. D.; Zhou, C. W.; Marks, T. J.; Janes, D. B. *Nat. Nanotech.* **2007**, *2* (6), 378−384.
(29) Lopes, W. A.; Jaeger, H. M. *Nature* **2001**, *414* (6865), 735−738.
(30) Aizawa, M.; Buriak, J. M. *J. Am. Chem. Soc.* **2005**, *127* (25), 8932−8933.

(31) Darling, S. B.; Yufa, N. A.; Cisse, A. L.; Bader, S. D.; Sibener, S. J. *Adv. Mater.* **2005**, *17* (20), 2446−2450.
(32) Zhang, Q. L.; Xu, T.; Butterfield, D.; Misner, M. J.; Ryu, D. Y.; Emrick, T.; Russell, T. P. *Nano Lett.* **2005**, *5* (2), 357−361.
(33) Chiu, J. J.; Kim, B. J.; Kramer, E. J.; Pine, D. J. *J. Am. Chem. Soc.* **2005**, *127* (14), 5036−5037.
(34) Bockstaller, M. R.; Lapetnikov, Y.; Margel, S.; Thomas, E. L. *J. Am. Chem. Soc.* **2003**, *125* (18), 5276−5277.
(35) Bockstaller, M. R.; Mickiewicz, R. A.; Thomas, E. L. *Adv. Mater.* **2005**, *17* (11), 1331−1349.
(36) Horiuchi, S.; Sarwar, M. I.; Nakao, Y. *Adv. Mater.* **2000**, *12* (20), 1507−1511.
(37) Kim, B. J.; Chiu, J. J.; Yi, G. R.; Pine, D. J.; Kramer, E. J. *Adv. Mater.* **2005**, *17* (21), 2618−2622.
(38) Kim, B. J.; Bang, J.; Hawker, C. J.; Kramer, E. J. *Macromolecules* **2006**, *39* (12), 4108−4114.
(39) Lin, Y.; Boker, A.; He, J. B.; Sill, K.; Xiang, H. Q.; Abetz, C.; Li, X. F.; Wang, J.; Emrick, T.; Long, S.; Wang, Q.; Balazs, A.; Russell, T. P. *Nature* **2005**, *434* (7029), 55−59.
(40) Zou, S.; Hong, R.; Emrick, T.; Walker, G. C. *Langmuir* **2007**, *23* (4), 1612−1614.
(41) Sohn, B. H.; Cohen, R. E. *J. Appl. Polym. Sci.* **1997**, *65* (4), 723−729.
(42) Deshmukh, R. D.; Buxton, G. A.; Clarke, N.; Composto, R. J. *Macromolecules* **2007**, *40* (17), 6316−6324.
(43) Zhang, Q. L.; Gupta, S.; Emrick, T.; Russell, T. P. *J. Am. Chem. Soc.* **2006**, *128* (12), 3898−3899.
(44) Laicer, C. S. T.; Chastek, T. Q.; Lodge, T. P.; Taton, T. A. *Macromolecules* **2005**, *38* (23), 9749−9756.
(45) Laicer, C. S. T.; Mrozek, R. A.; Taton, T. A. *Polymer* **2007**, *48* (5), 1316−1328.
(46) Chen, K.; Ma, Y. Q. *J. Chem. Phys.* **2002**, *116* (18), 7783−7786.
(47) Anastasiadis, S. H.; Russell, T. P.; Satija, S. K.; Majkrzak, C. F. *J. Chem. Phys.* **1990**, *92* (9), 5677−5691.
(48) Sau, T. K.; Murphy, C. J. *Langmuir* **2004**, *20* (15), 6414−6420.
(49) Pierrat, S.; Zins, I.; Breivogel, A.; Sonnichsen, C. *Nano Lett.* **2007**, *7* (2), 259−263.
(50) Petrova, H.; Juste, J. P.; Pastoriza-Santos, I.; Hartland, G. V.; Liz-Marzan, L. M.; Mulvaney, P. *Phys. Chem. Chem. Phys.* **2006**, *8* (7), 814−821.
(51) Dalsin, J. L.; Lin, L.; Tosatti, S.; Voros, J.; Textor, M.; Messersmith, P. B. *Langmuir* **2005**, *21*, 640−646.
(52) Kreibig, U.; Vollmer, M. *Optical Properties of Metal Clusters*; Springer-Verlag: Berlin, 1995.
(53) Gole, A.; Murphy, C. J. *Chem. Mater.* **2005**, *17* 1325−1330.
(54) Wang, C.; Ma, Z.; Wang, T.; Su, Z. *Adv. Funct. Mater.* **2006**, *16* 1673−1678.
(55) Sylvester-Hvid, K. O.; Mikkelsen, K. V.; Nymand, T. M.; Astrand, P. O. *J. Phys. Chem. A* **2005**, *109* (5), 905−914.
(56) Bandrup, J.; Immergut, E. H.; Grulke, E. A. *Polymer Handbook*, fourth ed.; Wiley-Interscience: New York, 1999.
(57) Jiang, X. C.; Brioude, A.; Pileni, M. P. *Colloid Surf., A* **2006**, *277* (1−3), 201−206.
(58) Pryamitsyn, V.; Ganesan, V. *Macromolecules* **2006**, *39* (24), 8499−8510.
(59) Kim, S. H.; Misner, M. J.; Xu, T.; Kimura, M.; Russell, T. P. *Adv. Mater.* **2004**, *16* (3), 226−231.
(60) Porter, D. A.; Easterling, K. E. *Phase Transformations in Metals and Alloys*; Chapman and Hall: London, 1981.

NL071908R